INSTITUTE OF PHYSICS PUBLISHING PLASMA PHYSICS AND CONTROLLED FUSION

Plasma Phys. Control. Fusion **48** (2006) 609–620 doi:10.1088/0741-3335/48/5/008

A simple plasma diagnostic based on processing the electrical signals from coaxial discharges

H Bruzzone[1], **H Acuña**[1], **M Barbaglia**[2] **and A Clausse**[2]

[1] Universidad de Mar del Plata and CONICET, Funes 3350, 7600 Mar del Plata, Argentina
[2] CNEA-CONICET and Universidad Nacional del Centro, 7000 Tandil, Argentina

Received 9 November 2005, in final form 19 February 2006
Published 31 March 2006
Online at stacks.iop.org/PPCF/48/609

Abstract

A technique for the determination of the inductance evolution in coaxial discharges based on measurements of the voltage between the electrodes and of the discharge current time derivative is presented and discussed. The technique is applied to measurements performed in a 5.7 kJ plasma focus device operating with deuterium filling in the 1–6 mbar range (which is the neutron yield range) and the obtained results are in good agreement with the expected evolution of a current sheet within the electrodes system.

1. Introduction

Plasma shocks can be magnetically driven during high current discharges in low-pressure gases, induced by an external electric circuit. Radial currents between two coaxial electrodes can be accelerated to velocities of the order of $10\,\mathrm{cm}\mu\,\mathrm{s}^{-1}$, thus being an effective method to transform potential energy into kinetic energy. Coaxial pulsed discharges are very economical devices not only for interesting basic plasma research but also because they are at the core of a number of industrial applications (Moreno *et al* 2002) ranging from tailored soft x-ray sources (Zakaullah *et al* 2000, Hussain S *et al* 2004) and soft x-ray microlithography (Lee *et al* 1998) to hard x-ray introspective imaging of metallic pieces (Moreno *et al* 2001, Venere *et al* 2001, Raspa *et al* 2004, Hussain *et al* 2005), neutron production and applications (Silva *et al* 2003, Tartaglione *et al* 2004) and plasma thrusters (Scheuer *et al* 2001) among others.

In spite of intense research efforts during the last 45 years, there are still a number of basic features that are waiting for clarification. Among the most important controversial issues is the role played by the breakdown and the physical mechanisms responsible for the radiation emissions.

Numerous plasma diagnostic techniques were developed in order to collect experimental data from the plasma during coaxial discharges (Bruzzone 1991 and 2001, Soto *et al* 2001, Silva *et al* 2002, Soto *et al* 2003, Moreno *et al* 2003, Hussain *et al* 2003). However, usually the direct measurement of plasma properties requires expensive instrumentation and sophisticated equipment. Therefore it is worthwhile to look for diagnostics of the plasma evolution during the discharge based on simple techniques. An interesting parameter of coaxial discharges (and more generally, in any symmetric discharge) is the gun inductance, whose analysis can render

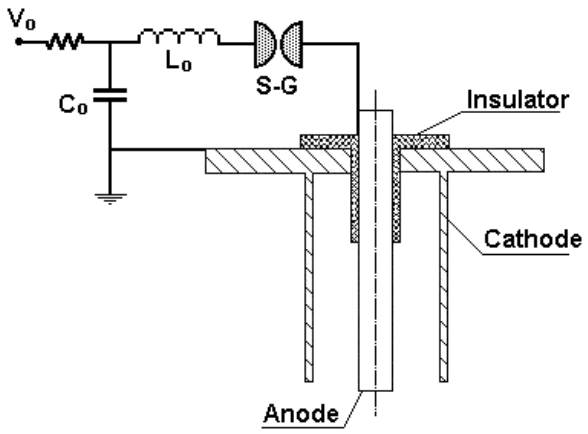

Figure 1. Diagram of the PF device and circuit.

information on plasma dynamics and can be used to validate numerical models. In this work, a technique to determine the inductance temporal evolution in plasma focus (PF) devices is presented. The technique only requires the measurement of the voltage between electrodes and the time derivative of the discharge current and can be used in any pulsed plasma forming electrical discharge provided that the plasma impedance can be assessed to be essentially inductive. Examples of the use of this technique are given for a specific PF device.

2. Experimental setup and procedure

A schematic of the PF device and circuit is given in figure 1. The bank capacity C_0 is 12.6 μF, the external inductance L_0 (measured with a short circuit on the insulator) is 40 nH (including 1.8 nH of the initial discharge on the insulator), the inner (r_1) and outer (r_2) radii are 1.8 cm and 3.6 cm, respectively, and their lengths (z) are 10 cm. The radius and length of the insulator (Pyrex glass) are 2.3 cm and 3.6 cm, respectively. The discharge chamber was evacuated down to less than 10^{-5} mbar for several minutes every time the gas was changed and then filled with fresh deuterium gas at the desired pressure. The pressure was measured by means of a capacitive manometer with an effective uncertainty of ± 0.05 mbar. Ten consecutive shots were done with the same gas filling, monitoring the stagnant-pressure changes (if any) from shot to shot. The voltage evolution between electrodes, $V(t)$, was measured with a calibrated fast resistive voltage divider and the time derivative of the discharge current, $\mathrm{d}I/\mathrm{d}t$, with a Rogowski coil. The signals were recorded using 2 ns-resolution digital oscilloscopes.

Special attention was paid to determine the component L_0' of the circuit inductance lying between the voltage divider and the plasma (see the equivalent circuit in figure 2). This value can be measured using several short-circuit shots, where the Rogowski and the voltage divider signals followed each other closely (i.e. the voltage between electrodes is simply the voltage drop on a constant inductance). A linear regression between both signals yielded a value (8.5 ± 0.2) nH, which agrees well with a geometric estimation of the connection's inductance. Discounting from this value 1.8 nH of the initial discharge on the insulator, the corresponding value of L_0' results as 6.7 nH.

Charging the capacitor bank at 30 kV ($\approx$ 5.7 kJ), ten shots were performed with initial filling pressures of 1.00, 2.00, 3.00, 4.00, 5.00 and 6.00 mbar. The magnitudes registered in every run were the pressure, p_0, before each shot, $V(t)$, $\mathrm{d}I/\mathrm{d}t$.

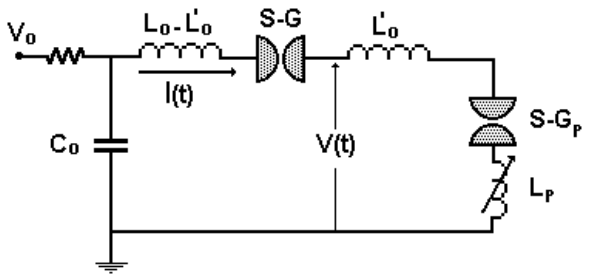

Figure 2. Diagram of the equivalent circuit for measurements. S–G_p represents the inter electrodes breaking gap and L_p is the gun inductance.

3. Results

After each shot, the filling pressure frequently changed and table 1 shows the evolution of p_0 from shot to shot. For all the initial filling pressures p_0 never increased more than 0.3 mbar in 10 shots. The minimum total pressure rise was at 2 mbar where p_0 reached 2.1 mbar in 10 shots. We did not observe any correlation between the pressure increase due to each shot and the neutron yield, that is, the pressure variation due to the shot does not deteriorate the yield in successive shots (actually the best shots at each initial p_0 were never the first ones). This observation suggests that the pressure increase is mainly due to deuterium outgassing from the walls and the electrodes. The latter is surely caused by the fact that the chamber was kept in high vacuum for many days before the experiment with a fair number of preliminary shots performed, repeatedly flushing the system with fresh deuterium gas.

Examples of $V(t)$ and $\mathrm{d}I/\mathrm{d}t$ signals obtained at 1 mbar, 3 mbar and 6 mbar are given in figures 3 (*a*), (*b*) and (*c*), respectively. In all the cases, $t = 0$ is defined at the start of $\mathrm{d}I/\mathrm{d}t$. It can be seen that the breakdown delay (i.e. the time difference between the start of $V(t)$ and that of $\mathrm{d}I/\mathrm{d}t$) diminishes as p_o increases. The high frequency oscillations appearing immediately after breakdown in both signals are due to resonances in the transmission lines connecting the bank with the electrodes (Bruzzone *et al* 1990). Although the start of $\mathrm{d}I/\mathrm{d}t$ is always accompanied by a drop in $V(t)$, there are important differences in the signal behaviour at different p_0. At 1, 2 and 3 mbar, $V(t)$ drops to a roughly constant value ($\approx$ 7 kV which lasts some 100 ns) and $\mathrm{d}I/\mathrm{d}t$ reaches its initial peak value ($\approx 7.5 \times 10^{11}$ A s^{-1}) immediately after the voltage drop. At higher p_0, the drop in $V(t)$ is smaller than 7 kV and becomes deep in the voltage curve which keeps rising afterwards until levelling around 7 kV. The latter is accompanied by a slower rise of $\mathrm{d}I/\mathrm{d}t$ to about 7.5×10^{11} A s^{-1}. The behaviour of both signals after the initial plateau is similar to that found in all PF devices, including the deep in $\mathrm{d}I/\mathrm{d}t$ and the accompanying peak in $V(t)$ characteristic of the pinch.

4. Analysis of the results

From the point of view of the electrical circuit, the evolution of the current sheet (CS) bridging the electrodes (i.e. run down towards the open end, convergence to the axis and final pinch formation) can be described as a time dependent inductance, $L_p(t)$, as shown in figure 2. In principle $L_p(t)$ can be determined from the measured values of $V(t)$ and $\mathrm{d}I/\mathrm{d}t$, although this calls for some discussion. Two different 'switches' exist in the circuit: the external spark-gap (SG) and the breakdown action within the gun electrodes (SG_p). The physical processes leading to the breakdown in the gun have been discussed elsewhere (Bruzzone and Vieytes 1993). Here we simply remind that, using general principles of electric circuit theory, the

Table 1. Experimental log.

# Shot	p_o (mbar)	L_{coax} (nH)	$t_c(\mu s)$	ΔL_p (nH)	I_p (kA)
1	1.00	—	—	—	440
2	1.10	10.8	1.14	5.8	433
3	1.15	—	—	—	431
4	1.20	9.9	1.14	5.7	441
5	1.20	—	—	—	458
6	1.20	10	1.15	4.7	440
7	1.20	—	—	—	457
8	1.20	10	1.17	11.8	440
9	1.25	—	—	—	453
10	1.30	10.4	1.21	9	439
1	2.00	—	—	—	450
2	2.00	10.2	1.20	3.1	445
3	2.00	10.5	1.28	3.4	449
4	2.00	10.4	1.28	—	456
5	2.00	10.4	1.23	7.3	438
6	2.00	—	—	—	461
7	2.05	10.1	1.25	4.1	465
8	2.05	—	—	—	460
9	2.10	10.2	1.24	8	461
10	2.10	10.6	1.33	3	449
1	3.00	9.96	1.34	2.8	449
2	3.00	10	1.33	5	455
3	3.00	10	1.28	7.3	460
4	3.00	9.82	1.33	7.4	451
5	3.10	9.96	1.31	6.4	456
6	3.10	9.88	1.31	4.1	462
7	3.10	9.79	1.33	9	458
8	3.10	10	1.33	9	458
9	3.20	9.83	1.36	3.5	454
10	3.20	9.77	1.36	7.6	445
1	4.00	12.2	1.54	4	453
2	4.10	10.8	1.46	6.9	464
3	4.10	10.4	1.45	6.8	456
4	4.15	10.9	1.49	7.8	451
5	4.15	11.3	1.55	5.4	468
6	4.20	11.3	1.51	7.5	461
7	4.20	10.5	1.45	6.9	459
8	4.20	10.9	1.44	7.2	467
9	4.20	10.7	1.52	7.5	446
10	4.25	10.6	1.45	8.5	471
1	5.00	—	—	—	456
2	5.10	11.4	1.52	7	466
3	5.10	11.7	1.59	7.7	456
4	5.10	11.5	1.55	8.7	470
5	5.20	11.4	1.57	7.5	453
6	5.20	11.5	1.57	6.2	458
7	5.20	11.4	1.58	7.5	452
8	5.20	11.8	1.55	6.2	461
9	5.20	11.3	1.63	8	456
10	5.20	11.7	1.58	6.2	456
1	6.00	—	—	—	399

Table 1. continued.

# Shot	p_o (mbar)	L_{coax} (nH)	$t_c(\mu s)$	ΔL_p (nH)	I_p (kA)
2	6.05	11.7	1.60	5.7	460
3	6.10	12.0	1.59	5.4	467
4	6.10	12.4	1.57	6.2	474
5	6.15	10.5	1.68	3.2	455
6	6.20	11.8	1.67	6.6	462
7	6.20	11.9	1.63	6.7	473
8	6.20	12.2	1.53	6.4	461
9	6.20	10.6	1.61	6.5	468
10	6.30	11.0	1.68	4.2	457

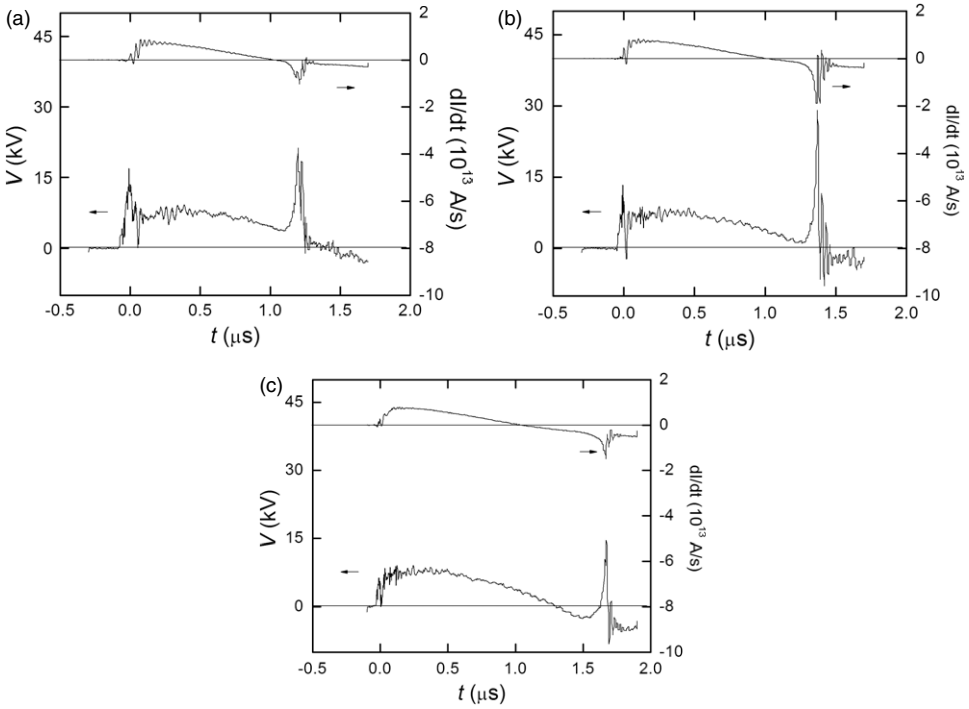

Figure 3. Typical voltage evolution and time derivative of the discharge current for (*a*) 1 mbar Deuterium pressure, (*b*) 3 mbar deuterium pressure and (*c*) 6 mbar deuterium pressure.

circuit can be said to be closed whenever $\mathrm{d}I/\mathrm{d}t$ attains the 'ideal' circuit initial peak value equal to V_0/L_0. In this context, to be closed means that the sum of the instantaneous resistances of both gaps drops below a certain fraction ($\sim$10%) of the external impedance, $(L_0/C_0)^{1/2}$. Therefore, after the first $\mathrm{d}I/\mathrm{d}t$ peak, the resistive component in $V(t)$ is much lower than the inductive voltage drop, leading to

$$V(t) = \frac{\mathrm{d}}{\mathrm{d}t}\left[\left(L_0' + L_\mathrm{p}(t)\right) I(t)\right], \tag{1}$$

which yields

$$L_\mathrm{p}(t) = \frac{\int_{t_0}^{t} V(t)\,\mathrm{d}t + (L_0' + L_\mathrm{p}(t_0))I(t_0)}{I(t)} - L_0', \tag{2}$$

where t_0 is the first peaking time of $\mathrm{d}I/\mathrm{d}t$.

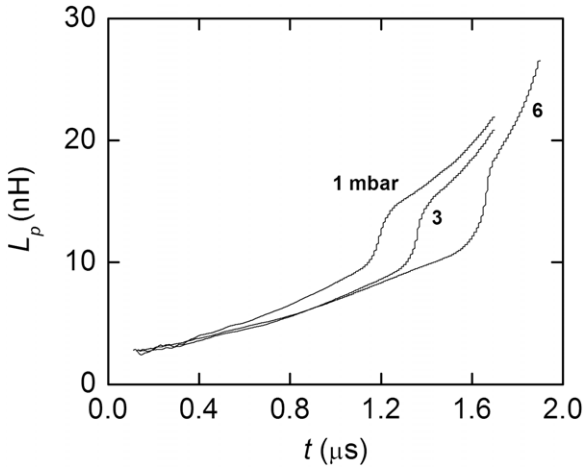

Figure 4. Evolutions of the gun inductance, $L_p(t)$ obtained for shot-6 in 1-mbar series, shot-6 in 3-mbar series and shot-4 in 6-mbar series (see table 1 for details). The errors are $\Delta L_{coax} \approx 0.2$ nH and $\Delta L_p \approx 0.4$ nH (see appendix).

An interesting observation is the fact that the ratio of the voltage in the divider and dI/dt 50 ns after t_0 averages (9.5 ± 0.2) nH, which is about 1 nH higher than $L'_0 + 1.8$ nH. This suggests that the initial current on the insulator is distributed in a 7 mm layer, accounting for the extra measured 1 nH. Actually, this kind of current distributions were measured with magnetic probes in similar devices (Bruzzone *et al* 1991). Taking the preceding discussion into account, a value $L_p(t_0) \approx 2.8$ nH was assumed in equation (2).

$L_p(t)$ was numerically calculated using the experimental signals $V(t)$ and $I(t)$. Figure 4 shows the results for particular shots at 1, 3 and 6 mbar. A general trend can be observed in all the curves: a roughly linear increase from the beginning up to a value which we call L_{coax} (about 10 nH), followed by a faster increase lasting about 100 ns and adding ΔL_p to the plasma inductance and finally a gentler rise but steeper than that in the initial stage. The same feature is found in all the shots, except in those without pinch, where the second stage is missed. Moreover, in figure 4 it can be seen that the starting time of the second stage (i.e. the sudden jump), t_c, increases with the filling pressure. It is worth mentioning that, to within a few tenths of nanoseconds, t_c coincides with the minimum of the 'focus' dip in dI/dt.

It should be stressed that the described behaviour of $L_p(t)$ is consistent with the standard picture of a moving CS in the coaxial set of electrodes. The initial stage corresponds to the travelling coaxial rundown, L_p at the end of the stage corresponding to the arrival at the open end of the electrodes. The arrival time increases with pressure because the CS runs slower at higher pressures. The second stage corresponds to the radial convergence of the CS up to the formation of a plasma column on the axis, and the third stage can be associated with the CS expansion outside the gun.

The complete set of measurements of $L_p(t)$ for 1, 3 and 6 mbar are given in figure 5. At 1 mbar (figure 5(*a*)), the initial-stage slopes spread considerably, the lowest slope values corresponding to the non-focusing shots. This behaviour suggests that there is a certain scattering in the speeds of the travelling CS during the coaxial stage, which would explain the corresponding scattering observed in the values of t_c. The inductance jumps in the second stage (when present) also show some scattering. The initial L_p slopes spreading is smaller at 3 mbar (figure 5(*b*)) than at 1 mbar (implying a more reproducible coaxial kinematics), although there is not much difference in the ΔL_p spreading at the second-stage. At 6 mbar

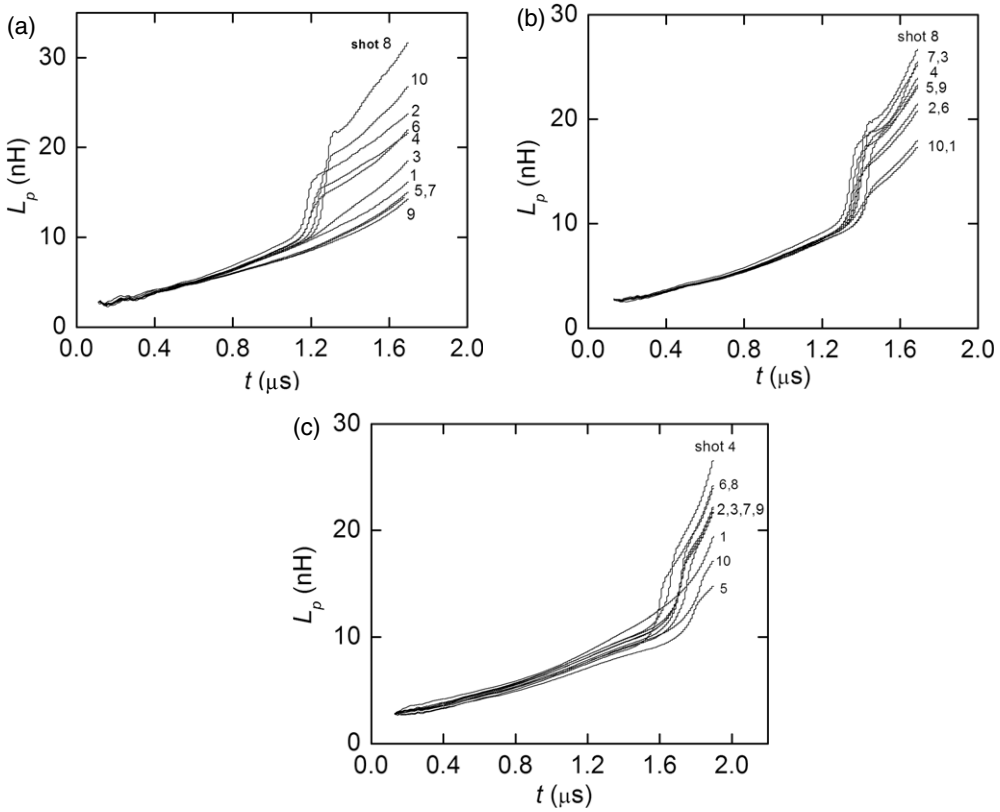

Figure 5. Plots of $L_p(t)$ for all the shots at 1 mbar (*a*), 3 mbar (*b*) and 6 mbar (*c*). The errors are $\Delta L_{coax} \approx 0.2$ nH and $\Delta L_p \approx 0.4$ nH (see appendix).

(figure 5(*c*)) the initial stage spreads vertically rather than in the slope, suggesting different initial $L_p(t_0)$ values, probably due to width differences of the initial CS. Measurements at other pressures (2, 4 and 5 mbar) showed similar intermediate features to those reported in figure 5. A summary of all measurements (L_{coax}, t_c, ΔL_p) is given in table 1.

A discussion on the uncertainties of these measurements is given in appendix 1, which shows that the main uncertainty sources are the Rogowski and voltage divider calibration constants, which together contribute in our case with a relative uncertainty of about 6%. Such uncertainty, however, affects the results just as an overall scale factor: it can shift up or down the whole curve but it does not affect the temporal profiles nor the differences observed between different shots. The uncertainty contributions which might affect temporal profiles and shot-to-shot variations are much smaller, typically less than 1%.

5. Discussion of the results

In order to validate the values of $L_p(t)$ determined with the experimental data, the results were compared with calculations based on geometrical estimates. The upper bound of L_{coax} is given by bridging the electrodes end with a thin and plane CS, that is

$$L_{coax}^{max} = \frac{\mu_0}{2\pi} z \ln\left(\frac{r_2}{r_1}\right) = 13.8\,nH. \tag{3}$$

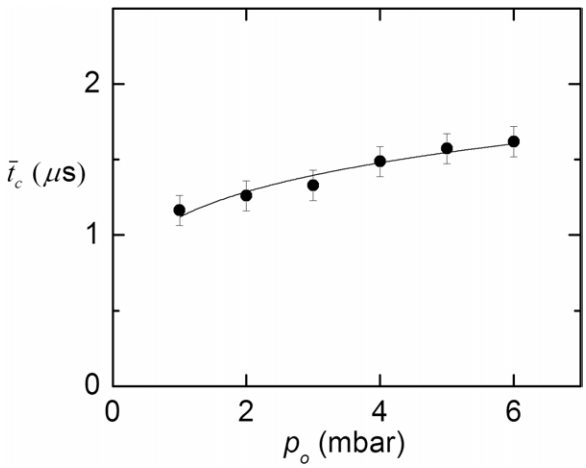

Figure 6. Pressure dependence of the average t_c. The full line is a numerical fit of the data points.

Since typical PF CSs have a tilted-bullet shape profile, the expected L_{coax} would be smaller than 13.8 nH, which is in agreement with the experiments.

On the other hand, the additional inductance added by the radial collapse can be roughly estimated adding a coaxial term formed by the pinch column with radius r_p, length d and a return current flowing at the external electrode radius. It is well known that in small energy PF devices r_p ranges between 1–2 mm and d ranges 1–2 cm. Consequently, ΔL_p should range between 3 and 7.3 nH, which is in reasonable agreement with the jumps measured in the second stage.

Figure 6 shows the pressure dependence of the average t_c. The curve drawn in this figure is an empirical correlation of the data points according to

$$\bar{t}_c = 1.1\ p_0^{0.2}. \tag{4}$$

In equation (4) $\bar{t}_c$ is in microseconds and p_0 is in millibars. Taking into account that, as mentioned before, t_c substantially coincides with the time of the dip in dI/dt, this time parameter can be understood as a measure of the focus time formation and hence as an overall estimate of the CS kinematics as a function of the pressure. The obtained pressure dependence deviates from the usual $p_0^{1/2}$ dependence of Mather-type PF (Mather 1971). However, reported experiments in low energy devices showed disagreements with the mentioned law (Silva *et al* 2004). Actually, the snow-plow model predicts that the axial speed of the travelling CS is proportional to $I(t)/p_0^{1/2}$, which in turn gives arrival times proportional to $p_0^{1/2}/\int_{t_0}^{t_c} I\,dt$, so that an additional pressure dependence can be expected from the integral of the current. In fact, we note that, as figure 7 shows, in our device the average peak current increases with the filling pressure, which increases the integral value as a function of p_0. Besides, an increase in p_0 implies an increase in the upper limit of the current integral determining the arrival time. It is therefore reasonable to expect as a net effect a softer dependence of t_c on p_0, as observed in the experiment.

6. Conclusions

A technique for assessing the evolution of the gun inductance in PF devices is presented. The assessment was applied to measurements taken on deuterium discharges in a small PF device,

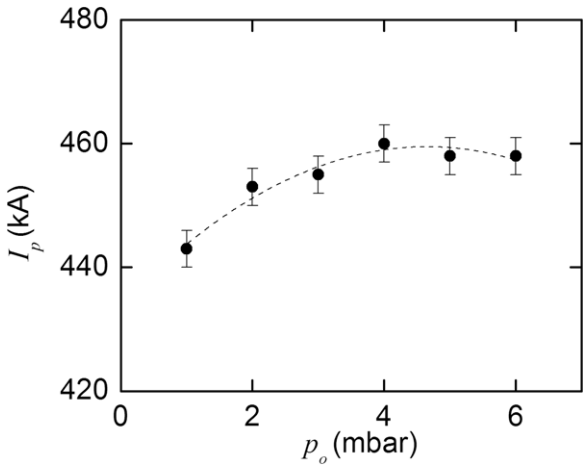

Figure 7. Pressure dependence of the peak current. The dotted line is a simple tendency line.

finding reasonable agreement with the expected overall behaviour. The resulting values can be used to reveal features of the plasma evolution during the discharge and can be used for making comparisons with theoretical predictions of different models (work in this direction is being conducted and will be presented elsewhere). In this context, it is interesting to comment on the t_c dependence on p_0, found in the particular set of measurements described in this work, because of its direct implications on PF scaling laws. In the light of the arguments given in the discussion of equation (4), it is clear that the particular exponent (0.2) found in this set of measurements has no special meaning, because such dependence should be expected to be dependent on the particular device used; however, it is also clear that a caveat should be put on the $p_0^{1/2}$ dependence for the focusing time sometimes used in scaling applications. It should be stressed, however, that this technique can be used in any PF device, including Filippov type ones and even in other pulsed plasma devices provided their plasma resistance can be shown to be small enough. This is so because the voltage between the electrodes is, in such cases, just the time derivative of the magnetic flux within the gun, which can always be expressed in terms of an inductance. A knowledge of the actual value of the fixed inductance L_0' in each particular device used is also necessary.

Acknowledgments

This work was supported by grants from the ANPCYT and CNEA-PLADEMA (Argentina) and the University of Mar del Plata. The experiments reported here were performed at the Institute of Plasma Physics of the University of Buenos Aires.

Appendix 1

The main measured quantities are

- the fixed external inductance in the voltage divider portion of the circuit $L_0' = (6.7 \pm 0.2)$ nH, disregarding the error in the estimation of the short circuit,
- the Rogowski coil coefficient, k_R, with 3% relative error,
- the Rogowski voltages, $V_R^i (i = 1, \ldots, 1020)$, with constant uncertainty ΔV_R,

- the voltage divider constant, k_{div}, with 3% relative error,
- the voltage in the voltage divider, $V^i_{\mathrm{div}}(i = 1, \ldots, 1020)$, with a constant uncertainty ΔV_{div},
- the digitalized time step $\Delta t = 2$ ns, with 1% relative error.

Using equation (2), the error in L_{p} can be written as

$$\delta L_{\mathrm{p}} = \delta Q - \delta L'_0, \tag{A1}$$

where δQ and $\delta L'_0$ are the absolute errors of the first and second terms of the right hand side of equation (2).

The assessment of δQ will be restricted to the later stages of the discharge, valid when

$$\int_{t_0}^{t} V(t)\mathrm{d}t > 5(L'_0 + L_{\mathrm{p}}(t_0))I(t_0) \tag{A2}$$

holds. This corresponds to $t > 500$ ns for all the shots, and in such cases one can write

$$\varepsilon Q = \varepsilon \left[\frac{\int_{t_0}^{t} V\mathrm{d}t}{I(t)} \right], \tag{A3}$$

where the operator ε means relative error.

Discretizing the expressions in the bracket of equation (A3) leads to

$$\int_{t_0}^{t} V(t)\mathrm{d}t = k_V \int_{t_o}^{t} V_{\mathrm{div}}(t)\mathrm{d}t \approx k_V \Delta t \sum_{i=n_0}^{n} V^i_{\mathrm{div}}, \tag{A4}$$

$$I(t) = k_{\mathrm{R}} \int_{0}^{t} V_{\mathrm{R}}(t)\mathrm{d}t \approx k_{\mathrm{R}} \Delta t \sum_{i=1}^{n} V^i_{\mathrm{R}}, \tag{A5}$$

where i is the step index, n_0 corresponds to $t = t_0$ ($n_0 \approx 60$), $i = 1$ corresponds to $t = 0$ and n corresponds to a generic time t.

Combining equations (A3) to (A5), and calculating the corresponding relative errors, yields

$$\varepsilon Q \approx \left[\varepsilon k_{\mathrm{div}} + \varepsilon k_V + \varepsilon \left(\sum_{i=n_0}^{n} V^i_{\mathrm{div}} \right) + \varepsilon \left(\sum_{i=1}^{n} V^i_R \right) \right]. \tag{A6}$$

Assuming Gaussian distributions for the voltage errors leads to

$$\begin{aligned} \varepsilon \left(\sum_{i=k}^{n} V^i_{\mathrm{div}} \right) &= \sqrt{(n-k)} \frac{\Delta V_{\mathrm{div}}}{\sum_{i=k}^{n} V^i_{\mathrm{div}}}, \\ \varepsilon \left(\sum_{i=1}^{n} V^i_R \right) &= \sqrt{n} \frac{\Delta V_R}{\sum_{i=1}^{n} V^i_R}. \end{aligned} \tag{A7}$$

The denominators in equation (A7) can be written as

$$\begin{aligned} \sum_{i=k}^{n} V^i_{\mathrm{div}} &= (n - n_0)\langle V_{\mathrm{div}} \rangle_{n-n_0}, \\ \sum_{i=1}^{n} V^i_R &= n\langle V_R \rangle_n, \end{aligned} \tag{A8}$$

where $\langle V_{\mathrm{div}} \rangle_{n-n_0}$ and $\langle V_{\mathrm{R}} \rangle_n$ are the voltages on the divider and the Rogowski averaged over the intervals n_0 to n and 1 to n, respectively.

It is important to stress that there is a conceptual difference between the error sources acting on Q. Those coming from the digitizer operation are statistical in nature, while those due to the calibration constants are fixed uncertainties. The uncertainties in k_{div}, k_V and L'_0 come from the difficulties involved in determining the values of these magnitudes, but there are no statistical variations involved. Hence, they essentially introduce systematic errors in $L_{\mathrm{p}}(t)$. On the contrary, the last two terms on the right-hand side of equation (A6) are statistical and their contribution to the total uncertainty varies with time. However, comparing the values of these two terms for all the shots shows that the voltage divider's contribution is always much smaller than 1% (note that the condition $t > 500\,\mathrm{ns}$ means $n > 250$), while that from the Rogowski coil can reach at most 1% due to the sign reversal of this signal at later times.

Combining equations (A1) to (A8), and taking into account the relative errors of each source, the estimated value of the error in L_{p} is

$$\delta L_{\mathrm{p}}(nH) \approx \pm[0.06(6.7 + L_{\mathrm{p}}(nH)) + 0.2]. \tag{A9}$$

In equation (A9), the upper bound of Q was estimated as L'_0–L_{p}.

Other sources of error are the uncertainty in the time t (corresponding to the index n), which is 0.02 $\mathrm{n}^{1/2}$ ns. Moreover, the values of t_{c}, L_{coax} and ΔL_{p} also contain additional uncertainties originated in the criteria used for their definition, resulting in $\Delta L_{\mathrm{coax}} \approx 0.2\,\mathrm{nH}$; $\Delta L_{\mathrm{p}} \approx 0.4\,\mathrm{nH}$ and $\Delta t_{\mathrm{c}} \approx 4\,\mathrm{ns}$.

References

Bruzzone H, Moreno C and Kelly H 1990 The effects of transmission lines and switching action on the electrical signals in a powerful capacitive discharge *IEEE Trans. Plasma Sci.* **18** 689–96

Bruzzone H, Moreno C and Kelly H 1991 Measurements of current sheets in plasmas with a finite-sized magnetic probe *Meas. Sci. Technol.* **2** 1195–200

Bruzzone H and Vieytes R 1993 The initial phase in plasma focus devices *Plasma Phys. Control. Fusion* **35** 1745–54

Bruzzone H and Martínez J 2001 Cinematic of the current sheet in a pulsed coaxial plasma source operated with uniform gas filling *Plasma Sources Sci. Technol.* **10** 471–7

Hussain A, Zakaullah M, Ali S, Bhatti S H, Waheed A 2003 X-ray enhancement from a plasma focus by inserting lead at the anode tip *Phys. Lett.* A **319** 181–7

Hussain S, Ahmad S, Khan M Z, Zakaullah M, and Waheed A 2004 Plasma focus as a high intensity flash x-ray source for biological radiography *J. Fusion Energy* **22** 195–200

Hussain S, Shafiq M, Ahmad R, Waheed A and Zakaullah M 2005 Plasma focus as a possible x-ray source for radiography *Plasma Sources Sci. Technol.* **14** 61–69

Lee S, Lee P, Zhang G, Feng X, Gribkov V, Liu M, Serban A and Wong T K S 1998 High rep rate high performance plasma focus as a powerful radiation source *IEEE Trans. Plasma Sci.* **26** 1119–26.

Mather J W 1971 Dense plasma focus *Methods of Experimental Physics* vol 9B, ed H Lovberg and H R Griem (New York: Academic) pp 187–249

Moreno C, Clausse A, Martínez J F, Llovera R and Tartaglione A 2001 Ultra fast x-ray introspective imaging of metallic objects using a plasma focus *Nukleonika* **46** S33–4 (Suppl 1)

Moreno C, Venere M, Barbuzza R, Del Fresno G, Ramos C, Bruzzone H, Florido P, González J and Clausse A 2002 Industrial applications of plasma focus radiation Braz. J. Phys. **32** 20–25

Moreno C, Casanova F, Correa G and Clausse A 2003 Experimental study and modeling of the plasma dynamics of magnetically driven shock waves in a coaxial tube *Plasma Phys. Control. Fusion* **45** 1989–99

Raspa V, Sigaut L, Llovera R, Cobelli P, Knoblauch P, Vieytes R, Clausse A and Moreno C 2004 Small plasma focus as a powerful hard x-ray source for ultrafast introspective imaging of moving metallic objects *Braz. J. Phys.* **34** 1696–99

Scheuer J T, Schoenberg K F, Gerwin R A, Hoyt R P, Henins I, Moses R W Jr Black D C and Mayo R M 2001 A magnetically-nozzled, quasi-steady, multimegawatt, coaxial plasma thruster *IEEE Trans. Plasma Sci.* **22** 1015–33

Silva P, Soto L, Sylvester G, Zambra M, Altamirano L, Bruzzone H, Clausse A and Moreno C 2002 Plasma focus driven by a capacitor bank of tens of joules *Rev. Sci. Instrum.* **73** 2583–90

Silva P, Moreno J, Soto L, Birstein L, Mayer R and Kies W 2003 Neutron emission from a fast plasma focus of 400 joules *Appl. Phys. Lett.* **83** 3269

Silva P, Soto L, Kies W and Moreno J 2004 Pinch evidence in a fast and small plasma focus of only tens of joules *Plasma Sources Sci. Technol.* **13** 329–32

Soto L, Esaulov V, Moreno J, Silva P, Sylvester G, Zambra M, Nazareno N and Clausse A 2001 Transient electrical discharges in small devices *J. Plasma Phys.* **8** 2572–8

Soto L, Silva P, Moreno J, Altamirano L and Clausse A 2003 Plasma motion observations in a very small plasma focus in the limit of low energy *Revista Mexicana de Física* **49** 140–2

Tartaglione C, Ramos C, Clausse A and Moreno C 2004 Detection of water by neutron scattering using a small plasma focus *Braz. J. Phys.* **34** 1756–8

Venere M, Moreno C, Clausse A, Barbuzza R and Del Fresno G 2001 Tomographic system based in plasma focus x-rays *Nukleonica* **46** 93–94

Zakaullah M, Alamgir K, Shafiq M, Sharif M, Waheed A and Murtaza G 2000 Low-energy plasma focus as a tailored x-ray source *J. Fusion Energy* **19** 143–57